(Received 11 October 2023, Accepted 18 December 2023, Scheduled 26 December 2023)

Circularly Polarized Antenna Array Using Filtering Phase Shifting Theory

Xin Guo[1, 2, *], Meiyu Du[1], Wen Wu[1], and Zhihong Feng[3, 4, *]

[1]*Key Laboratory of Near-Range RF Sensing ICs & Microsystems (NJUST), Ministry of Education Nanjing University of Science and Technology, Nanjing 210094, China*
[2]*State Key Laboratory of Millimeter Waves, Southeast University, Nanjing 210096, China*
[3]*National Key Laboratory of Solid-State Microwave Devices and Circuits, Shijiazhuang 050051, China*
[4]*Hebei Semiconductor Research Institute, Shijiazhuang 050051, China*

ABSTRACT: A new circularly polarized (CP) array using the filtering phase shifting theory is designed. First, a phase-designable filter is designed by adjusting the position of the transmission zero (TZ) of the doublet topology filter. Next, a phase-designable 3rd-order filtering antenna element can be obtained by using a stub-loaded resonator (SLR) as the physical structure of the doublet topology, and the patch is treated as the last resonating mode. Then, two 3rd-order filtering antenna elements with 90° phase difference are designed. Finally, by using the slot-coupled feed structure, four elements with phases of 0°, 90°, 180°, 270° are rotated sequentially to form a circularly polarized array. The measured results show that the impedance bandwidth is 8.1% (5.07–5.5 GHz); the axial ratio (AR) bandwidth is 6.7% (5.05–5.4 GHz); the maximum CP realized gain is 10.5 dBic; and the good filtering function is implanted.

1. INTRODUCTION

In modern communication systems, microstrip circularly polarized (CP) antenna has been extensively spread thanks to its merits of combating multi-path fading, insensitivity to linear polarization direction, and low profile. In addition, a lot of attention has been paid to the integration of the microwave functional components, which can reduce the size and transmission loss. Therefore, the integration of filter and circularly polarized antenna is worth studying.

To form the circularly polarized antenna, it is a common method to introduce perturbation elements, such as a truncated patch [1] or a patch with slot [2]. Based on this method and combined with the sequential rotation (SR) techniques in [3], the corresponding CP arrays can be generated in [4–7]. However, these CP antennas have narrow and undesignable axial ratio (AR) bandwidths, compared with their impedance bandwidths.

Parasitic elements and slot-coupled networks can be utilized to broaden the AR bandwidth of patch antennas. For instance, in [8] and [9], the AR bandwidth can be significantly improved by adding the parasitic patches. The above methods can also generate a circularly polarized array with wide AR bandwidth [10–12]. Nevertheless, this kind of CP antenna usually has relatively large size, high profile, or complicated structure, and has no filtering performance.

Currently, filter network is introduced to construct CP antennas. In [13], a broadband filtering CP antenna is formed by integrating two bandpass filtering linearly polarized components with 90° phase difference. In [14], two bandpass filter networks are designed to cooperate with a patch antenna, which successfully excite two orthogonal modes with equal magnitude and quadrature phase over the whole bandwidth. In [15], with the use of a novel dispersive delay line (DDL) with different in-band and out-of-band phase performances, a CP filtering patch antenna is obtained with good polarization isolation. To sum up, these CP filtering antennas have both the better CP property and filtering function over the passband than traditional design. However, these CP antennas are usually doubly-fed structures with a power divider in antenna element, which are not convenient enough for the array construction.

Herein, a novel CP filtering array is realized by using the proposed phase-designable filtering antenna elements with intrinsic 90° phase difference. Section 2 introduces the phase shifting theory by controlling the coupling matrix of the doublet topology filter. A preliminary design has been reported in [16]. In this article, the basic working mechanism, phase shifting trend and range, and detailed design method are demonstrated in depth. In Section 3, a patch antenna is treated as the last stage of the filtering network, by which two 3rd-order filtering antenna elements with 90° phase difference are designed. In Section 4, with the help of a wideband slot-coupled power divider, a four-element CP array is constructed based on the proposed two antenna elements with 90° phase difference. The last section is the measured result. The impedance bandwidth of the CP array is 8.1% (5.07–5.5 GHz); the AR bandwidth is 6.7% (5.05–5.4 GHz); and the CP maximal realized gain is 10.2 dBic. Moreover, a good filtering gain performance is observed.

* Corresponding authors: Xin Guo (guoxin@njust.edu.cn), Zhihong Feng (ga917vv@163.com).

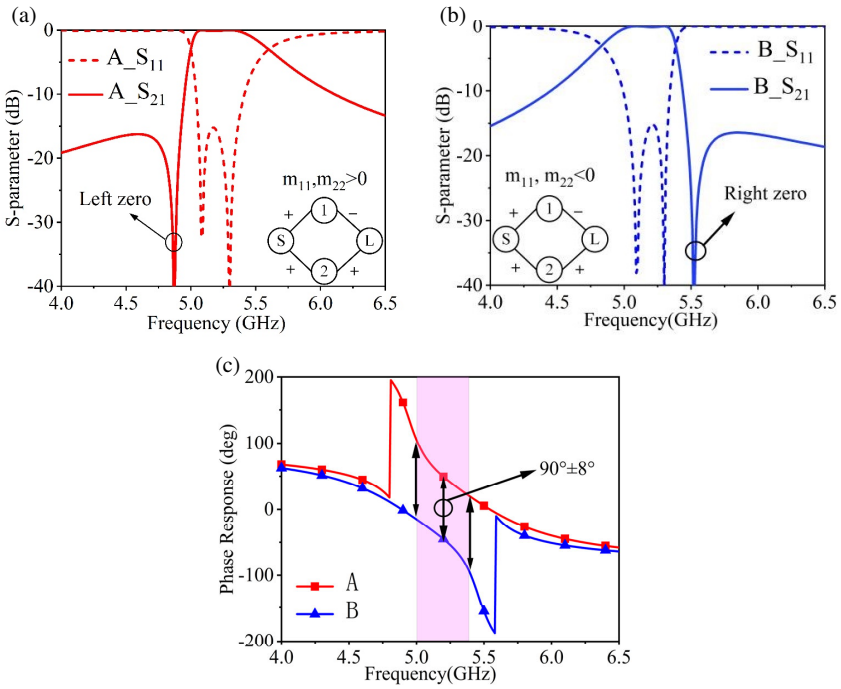

FIGURE 1. (a) Magnitude of Filter A with one left-side TZ. (b) Magnitude of Filter B with one right-side TZ. (c) Phase responses of Filter A and Filter B.

2. PHASE SHIFTING USING RECONFIGURABLE COUPLING MATRIX

2.1. Phase Shifting Phenomenon

This section demonstrates the phase shifting phenomenon of bandpass filter with the same topology but different coupling matrixes. Here, takes the simplest doublet topology as the example. The doublet with various matrix designs will produce different filtering magnitude responses. For example, in Fig. 1(a), the left transmission zero (TZ) response is generated. There are two in-band poles and one left out-of-band TZ. The coupling matrix m_a of this case is displayed as $[m_a]$, and the filter is labeled as Filter A.

$$[m_a] = \begin{bmatrix} 0 & m_{s1} & m_{s2} & 0 \\ m_{s1} & m_{11} & 0 & m_{1L} \\ m_{s2} & 0 & m_{22} & m_{2L} \\ 0 & m_{1L} & m_{2L} & 0 \end{bmatrix} \tag{1}$$

If the signs of m_{11} and m_{22} are changed at the same time, a new filter as in Fig. 1(b), in which the position of TZ is moved from below to above the passband, is obtained. The new coupling matrix of doublet topology is written as $[m_b]$, and the filter is labeled as Filter B.

$$[m_b] = \begin{bmatrix} 0 & m_{s1} & m_{s2} & 0 \\ m_{s1} & -m_{11} & 0 & m_{1L} \\ m_{s2} & 0 & -m_{22} & m_{2L} \\ 0 & m_{1L} & m_{2L} & 0 \end{bmatrix} \tag{2}$$

The two filters have the same center frequency and bandwidth. Besides, their TZs are symmetric with the center frequency.

Figure 1(c) shows the phase responses of Filter A and Filter B. It can be observed that the phase responses of these two filters are also symmetric with the center frequency. Specially, there are obvious phase jumps of 180° at the locations of the TZs. Hence, a phase difference is created at the center frequency introduced by the different phase jump positions. That is, one pair of coupling matrixes with symmetric TZs will produce a phase difference.

2.2. Phase Shifting Theory

This section demonstrates the phase shifting theory of doublet topology filters with different coupling matrixes. The transmission parameter S_{21} of the topology can be calculated by the coupling matrix $[m]$ following [17].

$$S_{21} = -2j[A]^{-1}_{4,1} \tag{3}$$

where $[A]^{-1}_{i,j}$ denotes the i^{th} row and j^{th} the column element of $[A]^{-1}$. The matrix $[A]$ is given by

$$[A] = [m] + \Omega[U] + j[q] \tag{4}$$

$[U]$ is a 4×4 identity matrix, except for $[U]_{1,1} = [U]_{5,5} = 0$; $[q]$ is a 4×4 matrix with all zeros, except that $[q]_{1,1} = [q]_{4,4} = 1$; Ω is the normalized frequency variable; $[m]$ is the 4×4 coupling matrix of the doublet topology filter. The phase response of filter can be calculated as Equation (5) at the bottom of this page.

$$\varphi = \angle S_{21} = \arctan\left(\frac{\text{imag}(S_{21})}{\text{real}(S_{21})}\right)$$

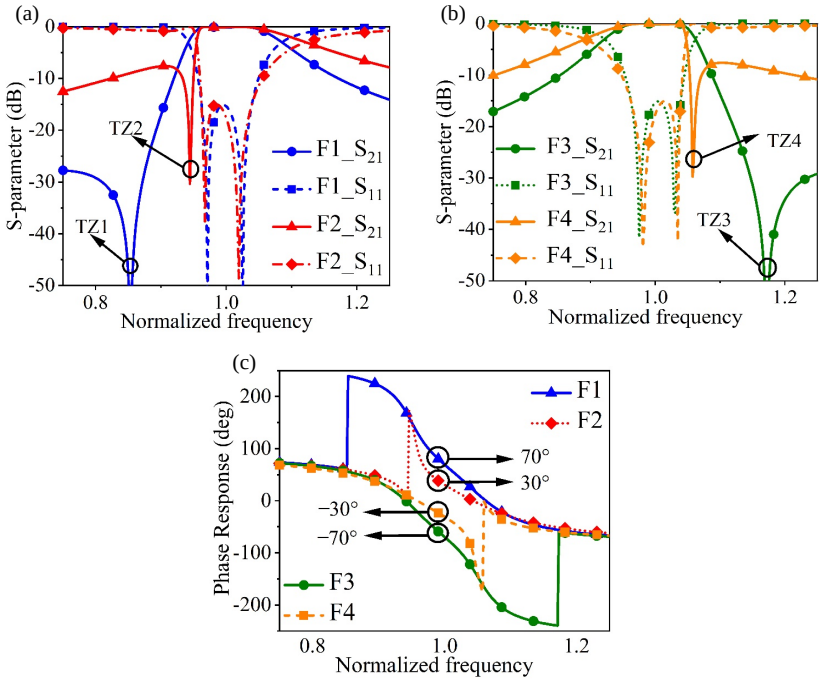

FIGURE 2. Filters with different TZs andphase responses. (a) Magnitude of filter F1 and filter F2. (b) Magnitude of filter F3 and filter F4. (c) Simulated phase responses of four filters in Figures 2(a) and 2(b).

TABLE 1. Parameters of different filters with the doublet topology but different matrix values.

Filters	Zero position	Phase response	m_{11}	m_{22}	m_{s1}	m_{s2}
F1	0.84	70°	−1.196	1.321	0.851	0.613
F2	0.95	30°	−0.839	1.231	1.1	0.355
F3	1.15	−70°	1.196	−1.321	0.851	0.613
F4	1.06	−30°	−0.839	1.231	1.1	0.355

$$= \arctan\left(\frac{\begin{array}{c} m_{s1}^2 m_{2L}^2 + m_{s2}^2 m_{1L}^2 - m_{11}m_{22} \\ -2m_{S1}m_{S2}m_{1L}m_{2L} \end{array}}{m_{22}m_{1L}^2 + m_{11}m_{2L}^2 + m_{22}m_{S1}^2 + m_{11}m_{S2}^2}\right) \quad (5)$$

In Equation (5), imag (S_{21}) and real (S_{21}) are the imaginary and real parts of S_{21}, respectively. The relationship of the imaginary and real parts of S_{21} between the coupling matrixes $[m_a]$ and $[m_b]$ can be calculated using Equation (5). The real part is the denominator of Equation (5), and the imaginary part is the numerator of Equation (5). The result can be seen as:

$$\begin{cases} \text{real}\left(S_b\left(2,1\right)\right) = -\text{real}\left(S_a\left(2,1\right)\right) \\ \text{imag}\left(S_b\left(2,1\right)\right) = \text{imag}\left(S_a\left(2,1\right)\right) \end{cases} \quad (6)$$

Hence, the phase relationship of matrixes $[m_a]$ and $[m_b]$ is shown as:

$$\varphi_b = -\varphi_a \quad (7)$$

According to the above analysis, a theoretical conclusion for this topology is that changing the position of TZ can change the phase response.

Next, the relationship between the phase response and TZ position of the proposed filter is studied numerically. Figs. 2(a), 2(b), and 2(c) display the magnitude and phase response of the filters with different prespecified TZs, and the coupling matrixes corresponding to those filters are shown in Table 1. Filters F1 and F2 in Fig. 2(a) correspond to the filters F3 and F4 in Fig. 2(b), respectively, as their coupling matrixes correspond to each other except for the opposite m_{11} and m_{22}. Their simulated phases have the opposite signs, thus the phase differences are shown. As shown in Figs. 2(a) and 2(c), the phase is positive when the TZ is at the left. And it decreases as the left TZ moves from far to near. Specifically, when the TZ is shifted from normalized frequency 0.84 to 0.95, the phase changes from 70° to 30° at the center frequency. As symmetry, in Figs. 2(b) and 2(c), the phase is negative when the TZ is at the right. And its absolute value decreases as the right TZ moves from far to near. Specifically, when the TZ is shifted from normalized frequency 1.15 to 1.06, the phase changes from −70° to −30° at the center frequency. In conclusion, as shown in Fig. 2(c), the phase at center frequency can be tuned from 70° to −70°, when the TZ is moved from the far left to far right within the achievable ranges.

According to the analysis above, we can design two filters with 90° phase difference. The coupling matrix of the filter

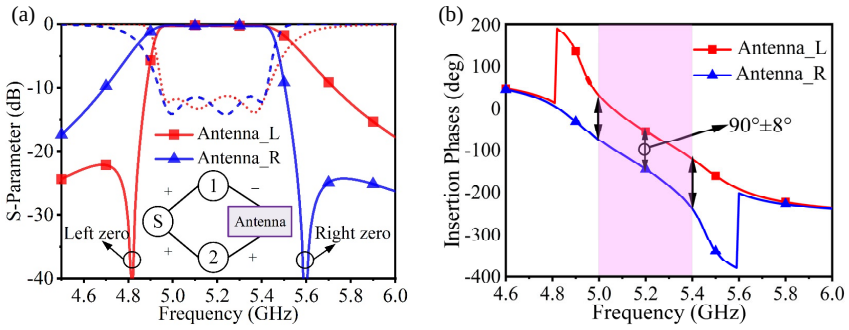

FIGURE 3. Filtering antenna element. (a) Magnitude responses of filtering antennas. (b) Phase responses of filtering antennas.

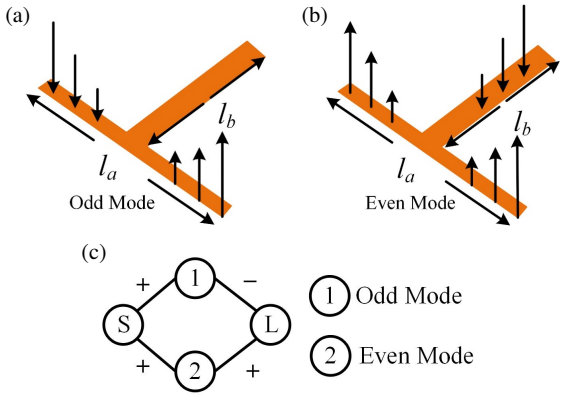

FIGURE 4. (a) Electric field distribution of SLR in odd-mode. (b) Electric field distribution of SLR in even-mode. (c) Corresponding doublet topology.

with 45° phase is designed as:

$$[m_A] = \begin{bmatrix} 0 & 1 & 0.456 & 0 \\ 1 & -1.002 & 0 & -1 \\ 0.456 & 0 & 1.288 & 0.456 \\ 0 & -1 & 0.456 & 0 \end{bmatrix} \quad (8)$$

The coupling matrix of the filter with $-45°$ phase response is designed as:

$$[m_B] = \begin{bmatrix} 0 & 1 & 0.456 & 0 \\ 1 & 1.002 & 0 & -1 \\ 0.456 & 0 & -1.288 & 0.456 \\ 0 & -1 & 0.456 & 0 \end{bmatrix} \quad (9)$$

Figure 1(c) is the phase responses of the above coupling matrixes $[m_A]$ and $[m_B]$. It can be observed that their phase responses are symmetric with the center frequency, and they have 90° phase difference at the center frequency. Therefore, the simulation results are consistent with the theory.

3. SIMULATION AND EXPERIMENT

In this section, two filtering antenna elements with 90° phase difference can be obtained by using the theory mentioned above. The center frequency is $f_0 = 5.2$ GHz, and the 10 dB return loss (RL) bandwidth is predefined as 8% (5–5.4 GHz). As shown in the inset of Fig. 3(a), the patch antenna is treated as the last stage resonator of the filtering network. Thus, the filtering antenna networks in Fig. 3(a) have three transmission poles and one TZ, which presents a 3rd-order filtering performance. In this way, compared with doublet topology, the networks of filtering antennas have the better selectivity and wider bandwidth. Fig. 3(b) is the phase response of the filtering antennas in Fig. 3(a), which is consistent with the above expectation.

To realize the doublet in physical structure, a stub-loaded resonator (SLR) is used. Its first two resonating modes are utilized to construct the doublet, and the field distributions of two modes are plotted in Figs. 4(a) and 4(b), respectively. In Fig. 4(a), when the odd mode is excited, the electric field is odd-symmetrical at two sides of l_a, and the coupling coefficients at the two sides are opposite. The stub is equivalent to be shorted, and the current mainly flows through the total of l_a, rarely through l_b. Hence, the frequency could be controlled by l_a. Similarly, in Fig. 4(b), when the even mode is excited, the electric field is even-symmetrical at two sides of l_a, and the coupling coefficients at the two sides are the same. The current mainly flows both through l_a and l_b. Hence, the frequency could be controlled by l_b, on the basis that l_a has been determined by the odd-mode frequency. In conclusion, the equivalent circuit model of this resonator can match the doublet, as shown in Fig. 4(c). Moreover, l_a controls m_{11}, and l_b controls m_{22} in the filter and phase design.

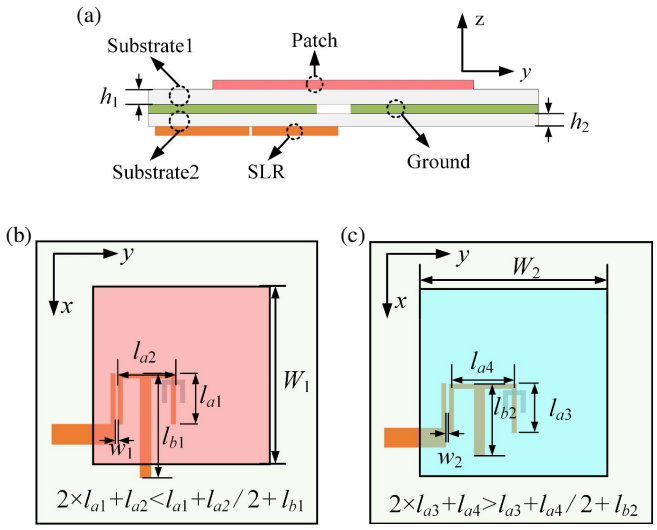

FIGURE 5. Geometry of proposed antenna elements with 90° phase difference. (a) Side view. (b) Top view of antenna with left TZ. (c) Top view of antenna with right TZ.

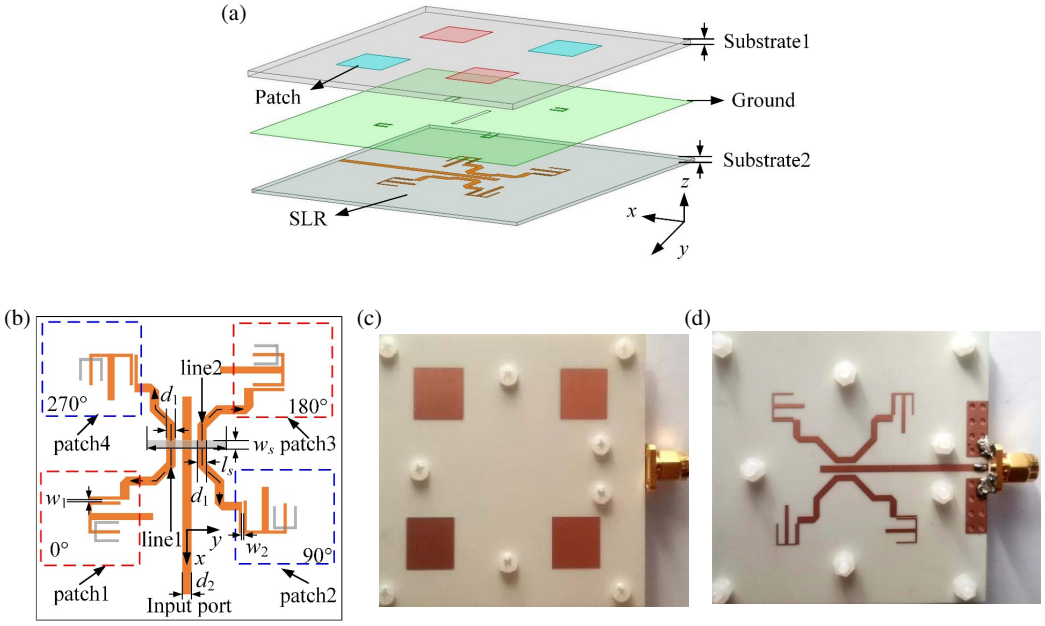

FIGURE 6. (a) 3D-view of proposed CP array. (b) Top view of proposed CP array. (c) Top view of physical structure. (d) Bottom view of physical structure.

Then, the structure of the proposed filtering antenna elements is designed as Fig. 5. Fig. 5(a) is the side view, and Figs. 5(b) and 5(c) are top view of the proposed filtering antennas with 90° phase difference. In Fig. 5(a), the patch is built on the top of substrate 1 which is Rogers RO4003C ($\varepsilon_r = 3.55$, $\tan\delta = 0.0027$) with the thickness (h_1) of 2 mm. The SLR is built on the bottom of substrate 2 which is Rogers RO4003C ($\varepsilon_r = 3.55$, $\tan\delta = 0.0027$) with thickness (h_2) of 0.813 mm. Between the two substrates, there is a U-shaped slot inserted in the ground plane. It is used to couple the electromagnetic energy from the feed to the radiating patch.

By designing the physical dimensions of the SLR and patch, filtering antennas with different TZs can be effectively generated, which is taken as the radiating elements with 90° phase difference of the CP filtering array. In Fig. 5(b), the SLR is folded for compactness, and l_a is divided into l_{a1} and l_{a2}. f_{odd} depends on the lengths of l_{a1} and l_{a2}, and f_{even} depends on the length of l_{b1} on the basis that the l_{a1} and l_{a2} have been determined by the odd-mode frequency, and the length or width of patch depends on the expected f. From the resonating condition, when $2\times l_{a1}+l_{a2}$ is smaller than $l_{a1}+l_{a2}/2+l_{b1}$, one left out-of-band TZ is obtained; when $2\times l_{a1}+l_{a2}$ is greater than $l_{a1}+l_{a2}/2+l_{b1}$, one right out-of-band TZ is obtained. Proper coupling strength could be optimized by tuning the coupling gaps, slot length and slot position. Afterwards, the filtering antennas with different TZs and 90° phase difference in Fig. 3

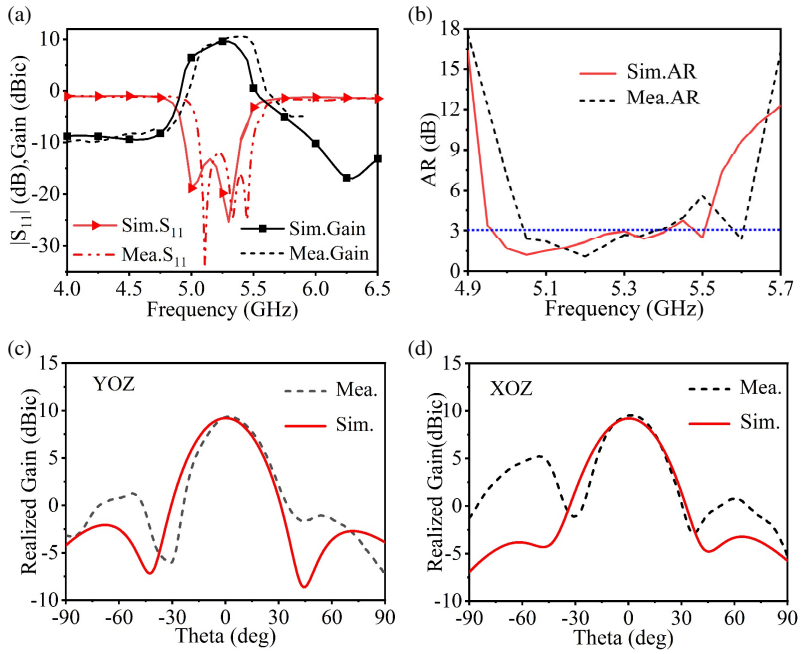

FIGURE 7. Simulated and measured results. (a) S parameters and realized gain. (b) AR. (c) Radiation pattern at 5.2 GHz in YOZ plane. (d) Radiation pattern at 5.2 GHz in XOZ plane.

can be physically obtained. The main parameters $l_{a1} = 5.8$, $l_{a2} = 5.5$, $l_{b1} = 10.5$, $W_1 = 12.6$, $w_1 = 0.2$, $l_{a3} = 5.8$, $l_{a4} = 6.9$, $l_{b2} = 8.4$, $W_2 = 12.5$, $w_2 = 0.25$, and the length of U-slot in Fig. 5(b) and Fig. 5(c) are 9.9 and 11.8, respectively (unit: mm).

4. CIRCULARLY-POLARIZED ANTENNA ARRAY

In this section, a 2×2 array using doublet fed antenna elements with 90° phase difference is designed as Fig. 6(a), and Fig. 6(b) illustrates the details. Here, $l_s = 15.2$, $w_s = 1.6$, $d_1 = 1.6$, $d_2 = 1.8$, line 1 = 34, line 2 = 34, $w_1 = 0.2$, $w_2 = 0.25$ (unit: mm). In Figs. 6(a) and 6(b), two antenna elements with 90° phase difference in Figs. 5(b) and 5(c) are taken as radiating elements. Figs. 6(c) and 6(d) are the top view and bottom view of the physical structure, respectively. A wideband slot-coupled power divider is designed to feed the antenna array. The slot etched on the ground plane is designed to couple the energy from the input transmission line to line 1 and line 2 which are parallel to the input transmission line. With the use of the slot, 0° phase difference will be generated at the same side of the slot, and 180° phase difference will be generated at different two sides of the slot. In conclusion, the phases of patches 1 and 2 are the same, and the phases of patches 3 and 4 are the same. Meanwhile, the phase between patches 1 or 2 and patches 3 or 4 is 180°.

By designing patches 1 and 2 as phase elements with 90° phase difference, as well as patches 3 and 4, four antenna elements with 0°, 90°, 180°, 270° phase response are rotated sequentially and form a circularly polarized array. The spacing between elements is $0.65\lambda_g$. The proposed 2×2 circularly polarized array is simulated by ANSYS HFSS. Fig. 7(a) shows the simulated and measured return losses and realized gains. As observed, the simulated impedance bandwidth is 8.7% (4.95–5.4 GHz), and the measured value is 8.1% (5.07–5.5 GHz). The right hand circular polarization (RHCP) peak simulated and measured gains are 9.7 dBic and 10.5 dBic, respectively. In addition, a good filtering performance is observed. Specifically, the simulated and measured gains drop sharply above 5.5 GHz and below 5 GHz, which is introduced by the elements designed by filter theory. Fig. 7(b) shows the simulated and measured ARs of 2×2 CP array. The simulated AR bandwidth is 8.7% (4.95–5.4 GHz), and the measured one is 6.7% (5.05–5.4 GHz). Within the bandwidths, the minimal AR values of simulation and measurement are 1.2 dB and 1.1 dB, respectively. Moreover, the AR is small in the bandwidth, and it increases sharply outside the bandwidth. Fig. 7(c) and Fig. 7(d) show the simulated and measured radiation patterns at 5.2 GHz of YOZ and XOZ planes, respectively. It needs to be pointed out that the impedance bandwidth and AR bandwidth are quantitatively designed, under the predefined 10 dB return loss (RL) bandwidth of 8%. They could also be narrower or wider, with other proper designs.

The comparison with other related CP antennas is tabulated in Table 2. First of all, from multifunctional aspect [5, 6, 10–12] do not have the filtering implanted function, and [13–15] have the filtering function. Compared with the truncated element using sequential rotation method, the proposed antenna has a controllable and designable AR bandwidth. Compared with parasitic element, the proposed one has more compact size, lower profile, and simpler structure. Compared with filtering antenna, the proposed element is single-fed, which is more convenient to construct an array and thus has a higher gain. In conclusion, the proposed structure has advantages including the filtering implanted, controllable and designable AR bandwidth, and simple structure. More importantly, as the element itself

TABLE 2. Comparison with other related CP antennas.

Ref.	Method	Feed	Layer	No. of Elements	Size (λ_0)	Gain (dBic)	S_{11} BW (%)	AR BW (%)	Filtering
[5]	Truncated+ sequential rotation	Single feed	1	4	$1.56 \times 1.56 \times 0.024$	13.59	15.4	5.3	No
[6]	Truncated+ sequential rotation	Single feed	1	4	$1.17 \times 1.17 \times 0.013$	7.5*	8*	4*	No
[10]	Parasitic	Single feed	2	4	$2.67 \times 2.67 \times 0.036$	10	44	26	No
[11]	Parasitic	Single feed	4	4	$1.5 \times 1.65 \times 0.12$	12.7	51	27	No
[12]	Parasitic	Single feed	1	4	$1.45 \times 1.45 \times 0.028$	12.5	15.9	11.8	No
[13]	Filter network and $\lambda/4$ transmission line	Double feed	3	1	$0.53 \times 0.53 \times 0.07$	5.2	12.5	12.5	Yes
[14]	Wilkinson power divider and $\lambda/2$ resonator	Double feed	2	1	$1.06 \times 1.06 \times 0.028$	5.8	10.3	8.8	Yes
[15]	Wilkinson power divider and dispersive delay line	Double feed	2	1	$0.7 \times 0.7 \times 0.026$	6.1	3.8	3.8	Yes
This work	Filter network	Single feed	2	4	$1.29 \times 1.29 \times 0.046$	10.4	8.1	6.7	Yes

*denotes the data is read from figures.

has phase control property, it will have tunable phase if the filtering performance is electrically reconfigurable. This design could be used to construct the beam scanning array or polarization reconfigurable array.

5. CONCLUSION

A 2×2 circularly polarized array by using transmission zero (TZ) adjustable filtering antenna elements with 90° phase difference is proposed. The phase shifting theory is analyzed, and the 90° phase shifting element can be quantitatively designed. Specially, there is no need to insert a $\lambda/4$ transmission line to form the 90° phase difference in the design, as it can be generated by using the filtering antenna element itself. Moreover, with the use of the filtering phase shifting method, the filtering function can be intrinsically implanted.

ACKNOWLEDGEMENT

This work was supported in part by the National Natural Science Foundation of China under Grant 61801223 and 62071235; and in part by the State Key Laboratory of Millimeter Waves under Grant K202327.

REFERENCES

[1] Sharma, P. C. and K. C. Gupta, "Analysis and optimized design of single feed circularly polarized microstrip antennas," *IEEE Transactions on Antennas and Propagation*, Vol. 31, No. 6, 949–955, Nov. 1983.

[2] Chen, W. S., C. K. Wu, and K. L. Wong, "Compact circularly polarised microstrip antenna with bent slots," *Electronics Letters*, Vol. 34, No. 13, 1278–1279, Jun. 1998.

[3] Huang, J., "A technique for an array to generate circular-polarization with linearly polarized elements," *IEEE Transactions on Antennas and Propagation*, Vol. 34, No. 9, 1113–1124, Sep. 1986.

[4] Hassan, A., F. Elhefnawi, A. Z. Elsherbeni, M. Hendi, and S. El-ramly, "Compact circularly polarized microstrip array antenna," *Microwave and Optical Technology Letters*, Vol. 53, No. 3, 604–609, Mar. 2011.

[5] Chen, A., Y. Zhang, Z. Chen, and S. Cao, "A Ka-band high-gain circularly polarized microstrip antenna array," *IEEE Antennas and Wireless Propagation Letters*, Vol. 9, 1115–1118, 2010.

[6] Lin, S.-K. and Y.-C. Lin, "A compact sequential-phase feed using uniform transmission lines for circularly polarized sequential-rotation arrays," *IEEE Transactions on Antennas and Propagation*, Vol. 59, No. 7, 2721–2724, Jul. 2011.

[7] Ye, S., J. Geng, X. Liang, Y. J. Guo, and R. Jin, "A compact dual-band orthogonal circularly polarized antenna array with disparate elements," *IEEE Transactions on Antennas and Propagation*, Vol. 63, No. 4, 1359–1364, Apr. 2015.

[8] Araki, K., H. Ueda, and T. Masayuki, "Numerical-analysis of circular disk microstrip antennas with parasitic elements," *IEEE Transactions on Antennas and Propagation*, Vol. 34, No. 12, 1390–1394, Dec. 1986.

[9] Gan, Z., Z.-H. Tu, Z.-M. Xie, Q.-X. Chu, and Y. Yao, "Compact wideband circularly polarized microstrip antenna array for 45 GHz application," *IEEE Transactions on Antennas and Propagation*, Vol. 66, No. 11, 6388–6392, Nov. 2018.

[10] Yang, S. S., R. Chair, A. A. Kishk, K.-F. Lee, and K.-M. Luk, "Study on sequential feeding networks for subarrays of circularly polarized elliptical dielectric resonator antenna," *IEEE Transactions on Antennas and Propagation*, Vol. 55, No. 2, 321–333, Feb. 2007.

[11] Nasimuddin, Z. N. Chen, and K. P. Esselle, "Wideband circularly polarized microstrip antenna array using a new single feed network," *Microwave and Optical Technology Letters*, Vol. 50, No. 7, 1784–1789, Jul. 2008.

[12] Ding, K., C. Gao, T. Yu, D. Qu, and B. Zhang, "Gain-improved broadband circularly polarized antenna array with parasitic patches," *IEEE Antennas and Wireless Propagation Letters*, Vol. 16, 1468–1471, 2016.

[13] Jiang, Z. H. and D. H. Werner, "A compact, wideband circularly polarized co-designed filtering antenna and its application for wearable devices with low SAR," *IEEE Transactions on Antennas and Propagation*, Vol. 63, No. 9, 3808–3818, Sep. 2015.

[14] Wu, Q.-S., X. Zhang, and L. Zhu, "Co-design of a wideband circularly polarized filtering patch antenna with three minima in axial ratio response," *IEEE Transactions on Antennas and Propagation*, Vol. 66, No. 10, 5022–5030, Oct. 2018.

[15] Wang, W., C. Chen, S. Wang, and W. Wu, "Circularly polarized patch antenna with filtering performance using polarization isolation and dispersive delay line," *IEEE Antennas and Wireless Propagation Letters*, Vol. 19, No. 8, 1457–1461, Aug. 2020.

[16] Du, M., X. Guo, and W. Wu, "Phase designable antenna element using filtering theory," in *2023 IEEE International Workshop on Electromagnetics: Applications and Student Innovation Competition (iWEM)*, 185–187, Harbin, China, Jul. 2023.

[17] Hong, J.-S. and M. J. Lancaster, *Microstrip Filters for RF/Microwave Applications*, John Wiley & Sons, New York, NY, USA, 2004.